ACS OMEGA

Open Access

http://pubs.acs.org/journal/acsodf

Article

First-Principles Calculations of the Phonon, Elastic, and Thermoelectric Properties of a Ti_2CO_2 Monolayer

She-Hui Yin, Xiao-Hong Li,* Rui-Zhou Zhang, and Hong-Ling Cui

Cite This: *ACS Omega* 2023, 8, 48549−48556

Read Online

ACCESS | Metrics & More | Article Recommendations

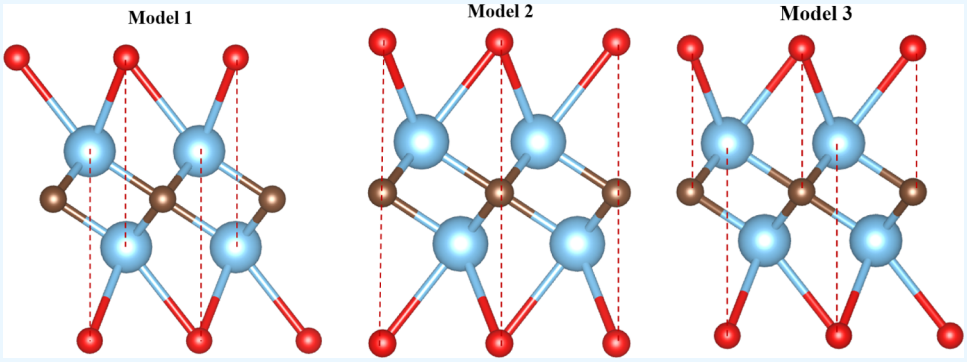

ABSTRACT: The phonon, elastic, and thermoelectric properties of Ti_2CO_2 are investigated by first-principles calculations. The dynamic and mechanical stabilities of Ti_2CO_2 are confirmed. The Ti_2CO_2 monolayer exhibits strong acoustic−optical coupling with the lowest optical frequency of 122.83 cm^{-1}. The TA mode originates from the contribution of Ti(XY) vibrations and has the largest gruneisen parameter at the Γ point; the LA mode has the main contribution of O(XY) and Ti(XY) vibrations and has the lowest gruneisen parameter at the *M* point. The analysis of the phonon spectrum indicates that the vibration contributions from C, O, and Ti atoms are mainly located in the low-, middle-, and high-energy regions, respectively. The Seebeck coefficient and electronic conductivity increase with increasing carrier concentration under room temperature. The analysis of mechanical properties shows that Ti_2CO_2 possesses a larger Young's modulus and bending modulus, which has a better ability to resist deformation. Thermal properties are further investigated.

1. INTRODUCTION

Two-dimensional (2D) materials have attracted great interest because of the superior performances caused by the reduced dimension since 2004.[1] Theoretical investigation indicates that 2D materials have superior properties such as high elastic stiffness, electronic properties, and energy storage characteristics.[2−6] Their atomically thin character also offers an excellent platform to design high-performance devices and develop next-generation technology.[7,8]

Graphene is a 2D material with superior mechanical and biological properties. It has wide applications in high-strength materials, energy storage, and transistors.[9−12] However, its zero-band gap character greatly hampers applications in highly integrated electronic components. Extensive efforts are focused on exploring and designing 2D materials beyond graphene. Recent experiments show that MXene with the formula of $M_{n+1}X_n$ belongs to a family of 2D materials and is obtained by removing A atoms from MAX materials.[13,14] F, O, and OH groups are often attached on the MXene surface during etching. So MXenes are expressed as $M_{n+1}X_nT_x$, where M is a transitional metal, T_x is a termination group, and X is a C/N atom. Compared with bare MXene, functionalized MXene shows many intriguing physicochemical properties and broadens its utilization in sensors,[15] supercapacitors,[16] and optoelectronics.[17]

MXenes with O and OH terminations are the most stable, and the OH group can change into O terminations at high temperature.[18] Therefore, the applications of O-functionalized MXenes are more promising when compared with MXenes with F and OH terminations. Ti_2CT_2 was successfully fabricated from the Ti_2AlC phase,[13] and Ti_2CO_2 was obtained by treating $Ti_2C(OH)_2$ at high temperature.[18]

Ti_2CO_2 has a semiconductor feature and is widely investigated. Our previous works investigated the influence of different O-vacancy concentrations and C-vacancy-line defects

Received: October 28, 2023
Revised: November 20, 2023
Accepted: November 24, 2023
Published: December 5, 2023

https://doi.org/10.1021/acsomega.3c08540
ACS Omega 2023, 8, 48549−48556

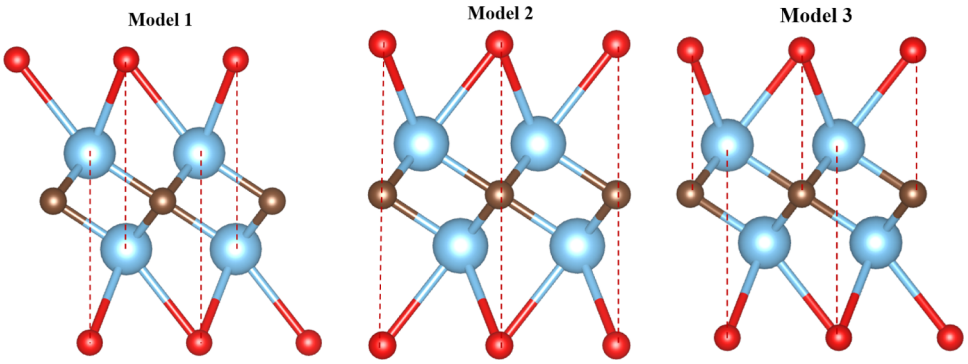

Figure 1. Three models for the Ti_2CO_2 monolayer.

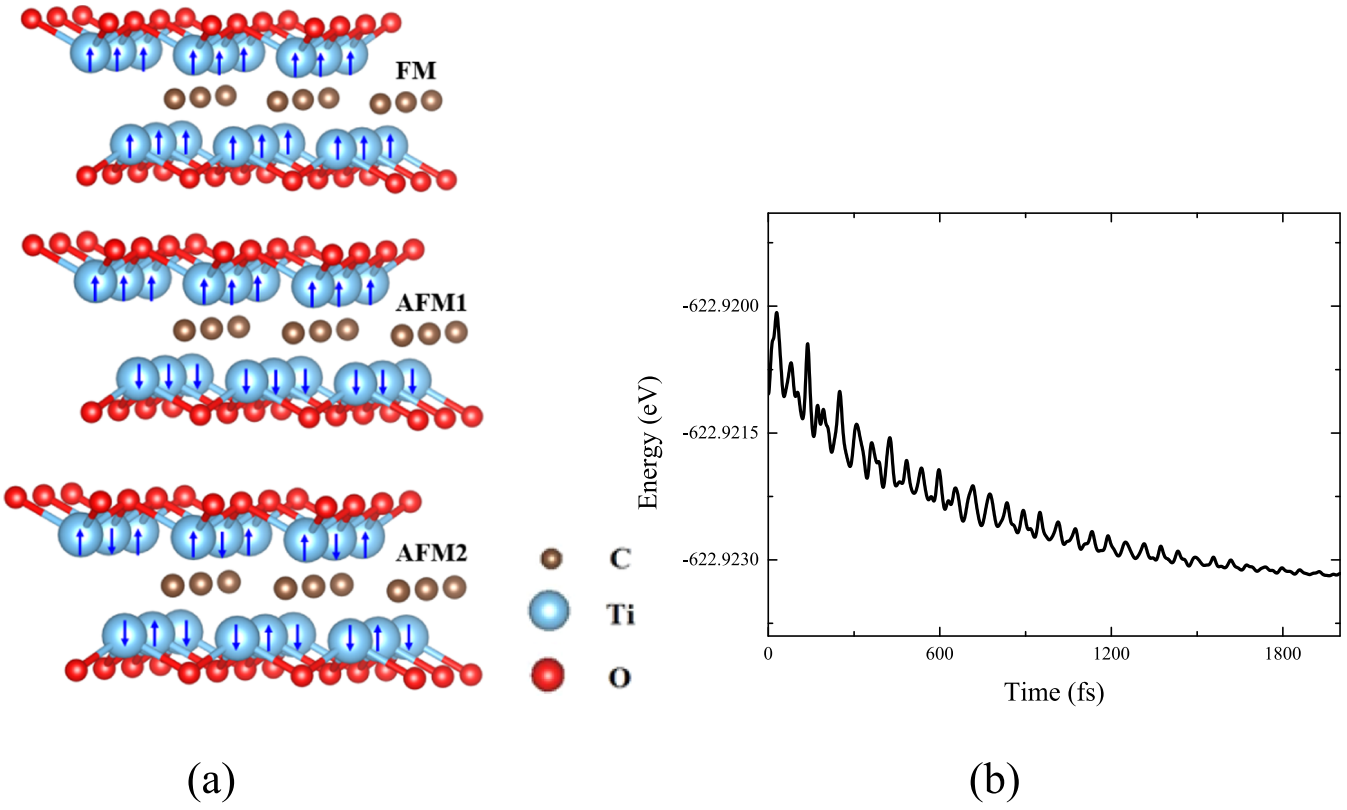

Figure 2. FM and AFM states of Ti_2CO_2 (a) and the energy of Ti_2CO_2 without magnetism during the simulation (b).

on electronic properties and quantum capacitance of Ti_2CO_2.[19,20] The adsorption of NH_3 on Ti_2CO_2 with a vacancy is further studied.[21] Ti_2CO_2 is an effective photocatalyst for CO_2 reduction.[22] Band-gap modulation of Ti_2CO_2 by strain is explored.[23] The electronic structure of Ti_2CO_2 is also studied by changing the layer thickness and strain.[24] Ti_2CO_x has the carrier mobility of 10^4 cm^2 V^{-1} s^{-1} experimentally.[25] To date, an investigation of the phonon, elastic, and thermoelectric properties of MXene with O termination is still lacking.

In this article, Ti_2CO_2 is selected to explore the phonon, elastic, and thermoelectric properties by first-principles calculations. This study can provide useful information for experimentalists to have an explicit physical mechanism of the related properties of MXenes.

2. COMPUTATIONAL METHODS

All calculations were performed by VASP code.[26] PAW pseudopotentials[27] and Perdew−Burke−Ernzerhof (PBE) functionals[28] were utilized. An energy cutoff of 700 eV was used. A large vacuum space of 25 Å was set to simulate the isolated monolayer. A 12 × 12 × 1 *k*-mesh was used for structural relaxation. The phonon calculation was performed by PHONOPY code[29] through the finite-displacement method.[30] A 4 × 4 × 1 supercell was constructed. The quasi-harmonic approximation (QHA) method[31] was used to investigate the lattice constant, bulk modulus, and thermal expansion of Ti_2CO_2 at different temperatures. Thermoelectric properties of the Ti_2CO_2 monolayer were further explored by using the BoltzTrap program.[32] A 25 × 25 × 1 *k*-mesh was used for transport coefficients of the Ti_2CO_2 monolayer.

https://doi.org/10.1021/acsomega.3c08540
ACS Omega 2023, 8, 48549−48556

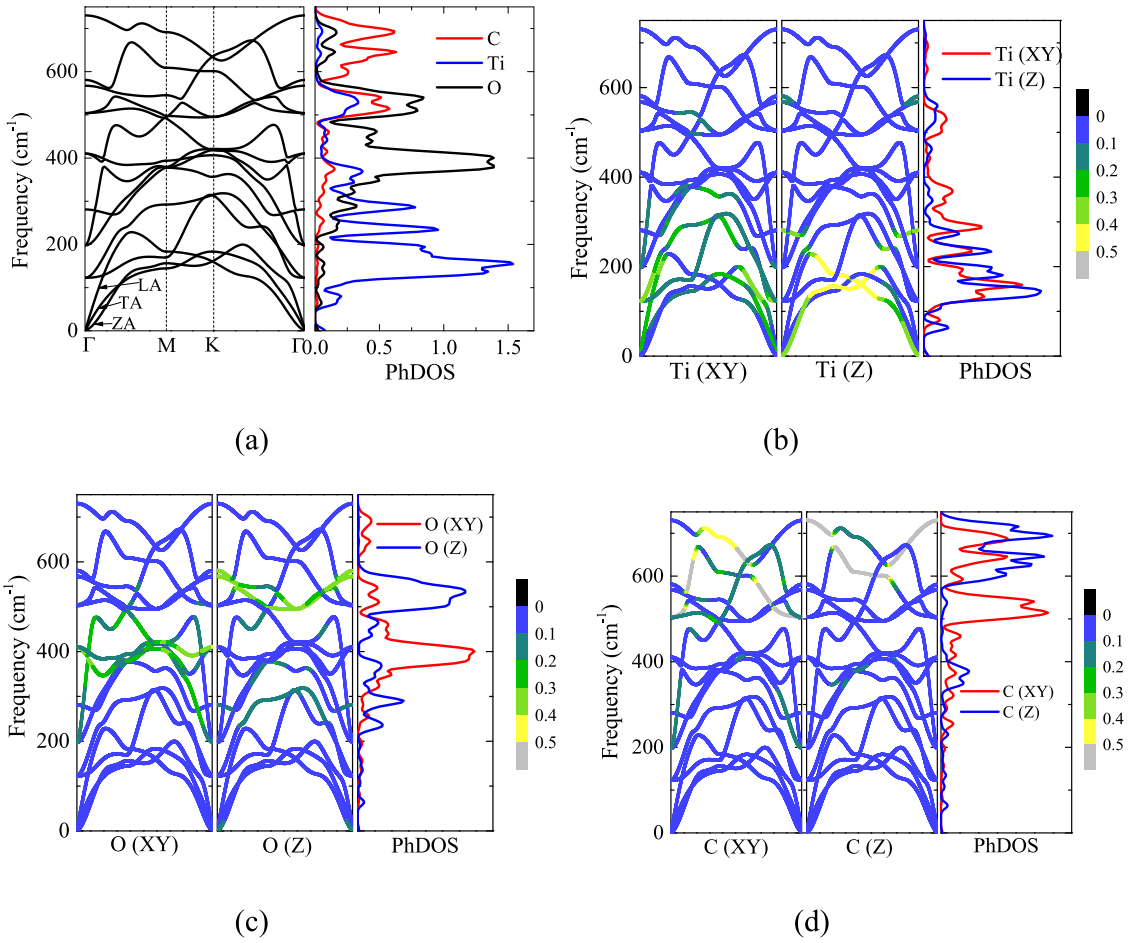

Figure 3. Phonon dispersions (a) and PhDOS and fat bands of the Ti_2CO_2 monolayer (b–d).

3. RESULTS AND DISCUSSION

3.1. Structure of the Ti_2CO_2 Monolayer. There are three possible configurations for the Ti_2CO_2 monolayer. That is, an O atom directly above a Ti atom as model 1, above a C atom as model 2, and model 3 with one O atom above a Ti atom and the other one above a C atom on each side. Figure 1 exhibits the three models. The result indicates that model 1 of the Ti_2CO_2 monolayer has the lowest energy, indicating that model 1 is the most stable for Ti_2CO_2. The lattice constant of Ti_2CO_2 is 3.045 Å, which is in accordance with ref 23.

The ferromagnetic (FM) and antiferromagnetic (AFM) states of Ti_2CO_2 are explored. First, for the FM state, the initial spins for Ti atoms all point in the same direction. Second, for the AFM state, we consider two possible magnetic orderings on Ti atoms, that is, AFM-stripy ordered (AFM1) and AFM-Neel (AFM2). Figure 2(a) plots the FM and AFM states of the Ti_2CO_2 monolayer. Results show that the energy of the system without magnetism (−400.1824 eV) is lower than those of FM (−400.1822 eV), AFM1(−400.18235 eV), and AFM2 (−400.18238 eV), which indicates that Ti_2CO_2 without magnetism is the most stable. The nonmagnetic character of the Ti_2CO_2 monolayer is in agreement with previous findings.[33−35] The following investigation is focused on Ti_2CO_2 without magnetism.

Molecular dynamics was performed by the DMOL3 program[36] to investigate the experimental stability of the Ti_2CO_2 monolayer. Figure 2(b) presents the total energy of Ti_2CO_2 without magnetism during simulation. The total energy of the Ti_2CO_2 monolayer oscillates around the same energy, indicating that Ti_2CO_2 is thermally stable at room temperature.

3.2. Phonon Spectrum. Figure 3 presents the phonon dispersion curves along the $\Gamma \rightarrow M \rightarrow K \rightarrow \Gamma$ and partial atomic phonon density of states (PhDOS) of the Ti_2CO_2 monolayer. From Figure 3(a), the totally positive frequencies confirm the dynamic stability of Ti_2CO_2. The acoustic modes are labeled ZA, TA, and LA, which are responsible mainly for heat transport in a narrow-gap semiconductor. ZA is the flexural acoustic mode with the atomic vibrations along the Z direction. LA and TA are the longitudinal and transverse acoustic modes, respectively, with the atomic vibrations both in the XY plane. The cross of TA and LA of Ti_2CO_2 is similar to that of the MoS_2 monolayer.[37]

Similar to other 2D systems,[38,39] the LA and TA modes of the Ti_2CO_2 monolayer exhibit linear dispersions near the Γ point and denote in-plane rigid-body motions, while its ZA mode denotes out-of-plane vibration and has quadratic dispersion. The highest optical phonon frequency of the Ti_2CO_2 monolayer is 730 cm^{-1}, slightly smaller than that for V_2CF_2.[40] The optical branches with low energy soften and overlap with the acoustic branches, which induces strong acoustic−optical interactions. The lowest optical mode boundary frequency of the Ti_2CO_2 monolayer is 122.83 cm^{-1}, which is larger than those of GeSe (64.19 cm^{-1}) and SnSe (52.04 cm^{-1}).[41] This indicates that the optical mode softening of Ti_2CO_2 is not so severe. From the PhDOS in

https://doi.org/10.1021/acsomega.3c08540
ACS Omega 2023, 8, 48549−48556

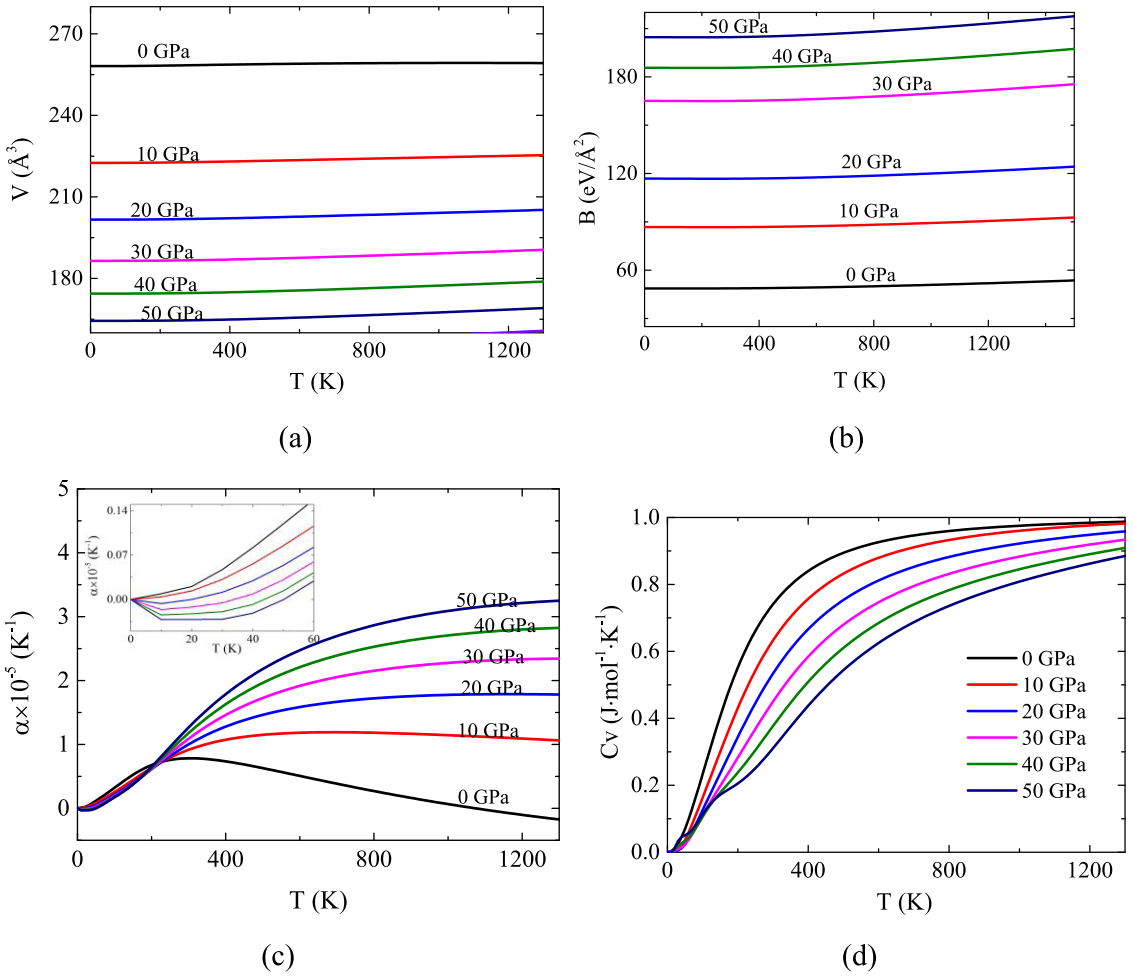

Figure 4. Volume (a), bulk modulus (b), thermal expansion (c), and isovolume heat capacity (d) at different temperatures and pressures. The inset in (c) is the thermal expansion coefficient at different temperatures and pressures in the energy range from 0 to 60 eV.

Figure 3(a), the contributions from C and O vibrations are located in the high- and middle-energy regions, respectively. The contributions from Ti vibrations are located in the low-energy region.

The fat bands for Ti(XY), Ti(Z), O(XY), O(Z), C(XY), and C(Z) vibrations are presented in Figure 3(b–d), along with their PhDOS. It is noted that the ZA mode mainly consists of Ti(Z) vibrations at the Γ point. O(XY) vibrations provide the increasing contribution of the fat band when getting away from the Γ point, which results in the covalent bonding characteristic. This is similar to graphene[42] and MoS_2.[37] The TA mode is mainly from Ti(XY) vibrations, and the LA mode has the main contribution of the O(XY) and Ti(XY) vibrations. C(XY) and C(Z) vibrations have the main contribution to the high-energy regions.

3.3. Thermal Properties. The thermal properties can provide information on materials about strength, phase stability, etc. Research shows that Ti_2CO_2 is stable at 1100 °C,[43] so the thermal properties of Ti_2CO_2 at temperature (T) up to 1300 K are studied at pressure (P) ranging from 0 to 50 GPa. Figure 4 presents the effect of T and P on the primitive cell volume (V), bulk modulus (B), thermal expansion coefficient (α), and heat capacity (C_V).

From Figure 4(a), the volume has little change with increasing temperature at 0 GPa. For a given temperature, the volume decreases with increasing pressure. At 300 K and 0 GPa, the V is 156.04 Å^3. Figure 4(b) presents the temperature dependence of B of the Ti_2CO_2 monolayer. At 0 GPa, B has a very slight change with increasing T. For a given temperature, B increases with increasing P, so Ti_2CO_2 has a strong ability to resist volume change. The B is 48.7 GPa at 300 K and 0 GPa.

Figure 4(c) presents the thermal expansion coefficient α of Ti_2CO_2. α increases sharply at low T and then decreases for a low pressure such as 0 and 10 GPa, while α gradually increases for a high pressure larger than 20 GPa. For a given T below 300 K, the higher the P, the lower the α. For a given T larger than 300 K, the higher the P, the higher the α. α is 1.6554 × 10^{-5} K^{-1} at 300 K, 0 GPa and α is 3.9 × 10^{-5} K^{-1} at 700 K, 0 GPa. They are larger than that of Ti_2AlC (1.19 × 10^{-5} K^{-1}).[44] The Ti_2CO_2 monolayer has a thermal contraction (negative α) below 50 K (the inset of Figure 4(c)) because of the activation of low-lying ZA modes. The Ti_2CO_2 monolayer changes to thermal expansion (positive α) with increasing temperature.

Figure 4(d) plots the heat capacity of Ti_2CO_2. One fully activated phonon branch will provide nearly 1.0 k_B to C_V at a high temperature and 0 GPa. At 300 K and 0 GPa, 74% of the phonon branches are activated. With increasing pressure, the activated phonon branches at 300 K decrease, with 63, 53, 45, 38, and 31% for 10, 20, 30, 40, and 50 GPa, respectively. At a lower temperature, C_V increases drastically and is proportional to T^3. For a given temperature, C_V decreases gradually as the pressure increases.

https://doi.org/10.1021/acsomega.3c08540
ACS Omega 2023, 8, 48549−48556

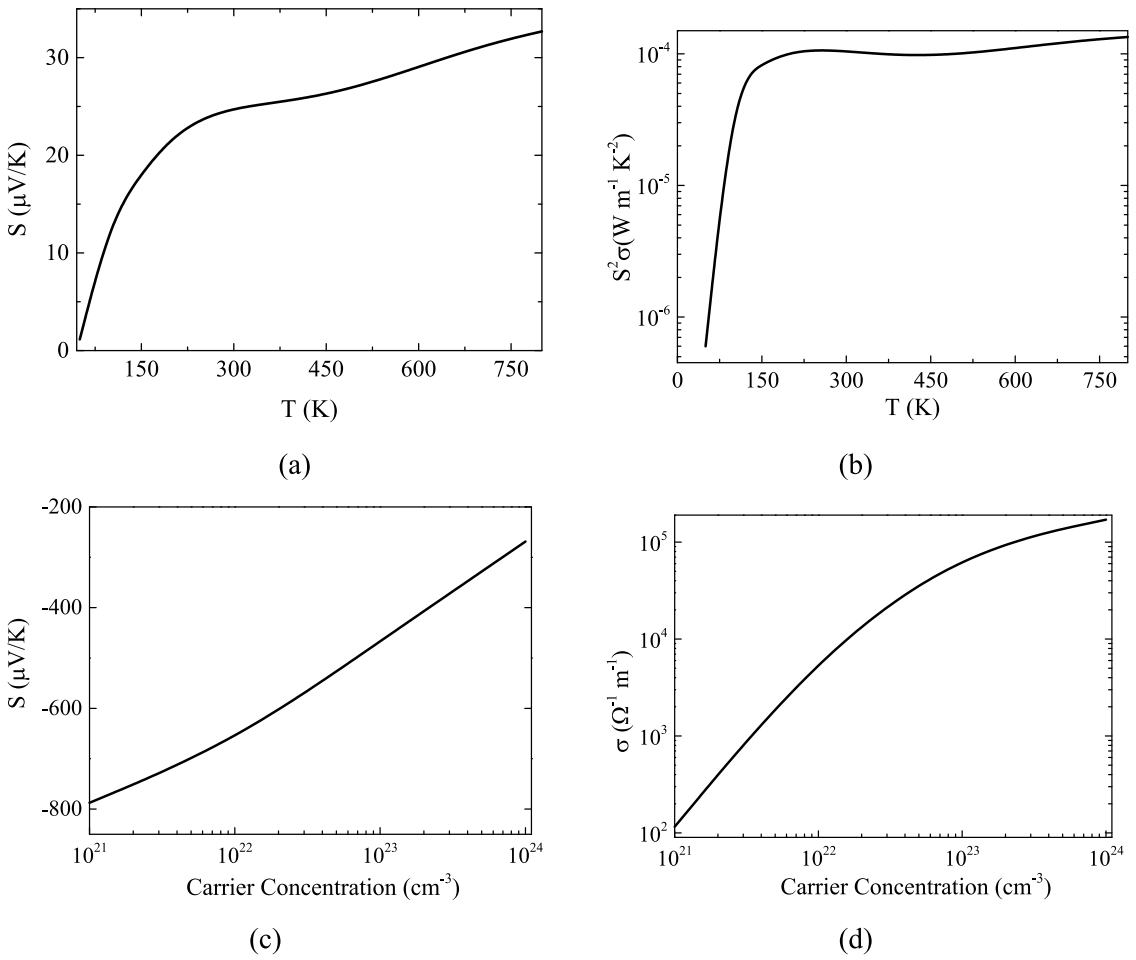

Figure 5. Thermoelectric properties of the Ti_2CO_2 monolayer: The Seebeck coefficient (a) and powder factor (b) as a function of temperature. The Seebeck coefficient (c) and electric conductivity (d) as a function of carrier concentration.

3.4. Thermoelectric Properties. Figure 5 presents thermoelectric properties such as the Seebeck coefficient S, electrical conductivity σ, and powder factor $S^2\sigma$. Figure 5(a) plots S under different temperatures at a fixed concentration of 1×10^{24} cm^{-3}. The Ti_2CO_2 monolayer shows p-type behavior because of the positive S. S has a positive correlation with T and increases with increasing T. However, S of Mo_2CF_2 has a negative correlation with T.[45] The electronic relaxation time τ of Ti_2CO_2 was estimated by Khazaei et al.[45] to be 10 fs. Figure 5(b) presents the powder factor $S^2\sigma$ of Ti_2CO_2 with a fixed concentration of 1×10^{24} cm^{-3}. The powder factor drastically increases at low temperatures and has an oscillating increase at temperatures larger than 200 K. Figure 5(c,d) presents S and σ at different carrier concentrations under 300 K. S and σ increase with increasing carrier concentration under room temperature, which is consistent with Appala's results.[46] No experimental data are available for the Ti_2CO_2 monolayer.

3.5. Elastic Properties. Elastic constants can reflect the stiffness and evaluate the mechanical behavior of materials against external stress within elastic limits. The mechanical stability and elastic properties of Ti_2CO_2 are explored by the elastic constant C_{ij}. C_{ij} is scaled by $C_{ij} = C_{ij,\text{cell}}\,(c/d_L)$,[47,48] where c is a lattice constant in the z-axis direction and d_L is the layer thickness. $C_{11} = C_{22}$ and $C_{66} = (C_{11} - C_{12})/2$ because of the hexagonal structure of Ti_2CO_2. The Born criteria of mechanical stability are $C_{11}^2 - C_{12}^2 > 0$ and $C_{66} > 0$ for a 2D material.[49] Young's modulus Y, Poisson ratio ν, shear modulus G, area modulus K, intrinsic strength σ_{int}, bending modulus D, and critical buckling strain ε_c are obtained by

$$Y = \frac{C_{11}C_{22} - C_{12}C_{21}}{C_{22}} \quad \nu = \frac{C_{12}}{C_{22}}$$
$$G_{xy} = C_{66} = \frac{C_{11} - C_{12}}{2} \tag{1}$$

$$K = \frac{Y}{3 \times (1 - 2\nu)} \quad \sigma_{\text{int}} \approx \frac{Y}{9} \quad D = \frac{Yh^2}{12(1 - \nu^2)}$$
$$\varepsilon_c = -\frac{4\pi^2 D}{YL^2} \tag{2}$$

For the hexagonal structure of Ti_2CO_2, $C_{11} = C_{22}$ and $C_{12} = C_{21}$. The calculated C_{11}, C_{12}, and C_{66} are 274, 85, and 94 N/M, respectively, which agree with Yorulmaz's results.[50] This shows that Ti_2CO_2 is mechanically stable. Larger C_{11} than C_{12} for Ti_2CO_2 indicates that a larger force is needed for axial compression when compared with shear and tensile deformations. Table 1 lists the Y, ν, G, K, σ_{int}, D, and ε_c of the Ti_2CO_2 monolayer.

Y of Ti_2CO_2 is 247.6 N/m, lower than that of graphene (342 N/m)[51] and h-BN (270 N/m),[52] but larger than that of MoS_2 (180 N/m).[53] This indicates that Ti_2CO_2 can resist deformation and has bitter rigidity, so it belongs to an incompressible material. ν of Ti_2CO_2 is 0.31, smaller than

https://doi.org/10.1021/acsomega.3c08540
ACS Omega 2023, 8, 48549−48556

Table 1. Y (N/m), ν, G (N/m), K (N/m), σ_{int} (N/m), D (eV), and ε_c of the Ti_2CO_2 Monolayer

parameter	value	parameter	value
Y	247.6	σ_{int}	27.5
ν	0.31	D	28.5
G_{xy}	94.5	ε_c	−0.067
K	217.5		

those of AlN, FAlNH, and HAlNH.[54] The bending modulus is important for 2D materials and has a great effect on potential flexible and stretchable electronic applications.[55] The D of graphene and MoS_2 are 1.2 and 9.61 eV, respectively.[56] The D value of Ti_2CO_2 is 28.5 eV, much larger than that of graphene and MoS_2. A larger bending modulus indicates that Ti_2CO_2 has a better ability to resist bending deformation.

3.6. Gruneisen Parameters. Gruneisen parameters (γ) can be used to describe the anharmonic interaction of a crystal, which is useful for analyzing the physical nature of lattice thermal conductivity (κ_L). Larger γ values indicate strong anharmonicity, which gives rise to low κ_L. Figure 6 presents the

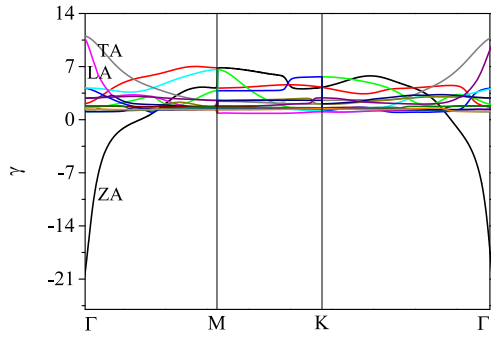

Figure 6. Gruneisen constant of the Ti_2CO_2 monolayer.

Gruneisen parameters (γ) of acoustic modes of the Ti_2CO_2 monolayer. It is noted that the ZA mode near the Γ point has large negative values, which is often found in other 2D systems[38,39,57] and consistent with the result of Sevik et al.[57] It can be attributed to the membrane effect:[39] contraction (expansion) always makes a membrane easier (harder) to bend, and then softens (stiffens) the Z-direction flexural vibration. The large negative values of the ZA mode near the Γ point also indicate that the acoustic branches of the Ti_2CO_2 monolayer are strongly anharmonic and crucial to the phonon transport in materials. The conversion of the positive γ(ZO) and negative γ(ZA) near the Γ point is due to the strong hybridization between XY and Z vibrations. The TA mode has the largest γ at the Γ point and the LA mode has the lowest γ at the M point.

4. CONCLUSIONS

In summary, we have theoretically performed the investigation of the phonon, elastic, and thermoelectric properties of Ti_2CO_2. The Ti_2CO_2 monolayer is dynamically stable because of the totally positive phonon frequencies. Results indicate that the highest optical phonon frequency of Ti_2CO_2 is 730 cm^{-1} and that its lowest optical frequency is 122.83 cm^{-1}. A strong acoustic−optical interaction is found. Through the analysis of PhDOS, O(XY) vibrations far away from the Γ point provide a larger contribution, which results in the covalent bonding characteristic. The TA mode has the largest γ at the Γ point and the LA mode has the lowest γ at the M point. The acoustic branches of Ti_2CO_2 are strongly anharmonic due to the large negative values of the ZA mode near the Γ point. The analysis of thermal properties indicates that the Ti_2CO_2 monolayer has a thermal contraction (negative α) below 50 K because of the activation of low-lying ZA modes and transforms into thermal expansion (positive α) with increasing temperature. A larger Young's modulus and bending modulus indicate that Ti_2CO_2 is more incompressible. Good thermoelectric properties demonstrate that Ti_2CO_2 has good potential for future application in the thermoelectric area.

AUTHOR INFORMATION

Corresponding Author

Xiao-Hong Li − *College of Physics and Engineering, Henan University of Science and Technology, Luoyang 471023, China*; orcid.org/0000-0003-2450-4476; Email: lorna639@yeah.net

Authors

She-Hui Yin − *Physical Teaching and Research of Fundamental Teaching Section, Henan Polytechnic Institute, Nanyang 473000, China*

Rui-Zhou Zhang − *College of Physics and Engineering, Henan University of Science and Technology, Luoyang 471023, China*

Hong-Ling Cui − *College of Physics and Engineering, Henan University of Science and Technology, Luoyang 471023, China*

Complete contact information is available at: https://pubs.acs.org/10.1021/acsomega.3c08540

Notes

The authors declare no competing financial interest.

ACKNOWLEDGMENTS

Key Scientific and Technological Projects in Henan Province (232102220023) is gratefully acknowledged.

REFERENCES

(1) Geim, A. K.; Novoselov, K. S. The rise of graphene. *Nat. Mater.* **2007**, *6*, 183−191.

(2) Wang, Y.; Tao, Y.; Zhang, Q.; Huang, R.; Gao, B.; Li, Z.; Li, G.; Hu, N. The structural, elastic, electronic, and optical properties of Janus Zr_2COT (T= S, Se, and Te) MXenes. *Solid State Commun.* **2022**, *354*, No. 114893.

(3) Mortazavi, B.; Shojaei, F.; Javvaji, B.; Rabczuk, T.; Zhuang, X. Outstandingly high thermal conductivity, elastic modulus, carrier mobility and piezoelectricity in two-dimensional semiconducting CrC_2N_4: a first-principles study. *Mater. Today Energy* **2021**, *22*, No. 100839.

(4) Su, T.; Lee, C. H.; Guo, S. D.; Wang, G.; Ong, W. L.; Cao, L.; Zhao, W.; Yang, S. A.; Ang, Y. S. 2D janus niobium oxydihalide NbOXY: Multifunctional piezoelectric semiconductor for electronics, photonics, sensing and sustainable energy applications. *Mater. Today Phys.* **2023**, *31*, No. 101001.

(5) Li, Z.; Zhang, J.; Zhou, B. Electric polarization related Dirac half-metallicity in Mn-trihalide Janus monolayers. *Phys. Chem. Chem. Phys.* **2020**, *22*, 26468−26477.

(6) Cui, X. H.; Li, X. H.; Jin, X. J.; Yan, H. T.; Zhang, R. Z.; Cui, H. L. Biaxial strain tunable quantum capacitance and photocatalytic properties of Hf_2CO_2 monolayer. *Appl. Surf. Sci.* **2023**, *616*, No. 156579.

https://doi.org/10.1021/acsomega.3c08540
ACS Omega 2023, 8, 48549−48556

(7) Cui, C.; Xue, F.; Hu, W. J.; Li, L. J. Two-dimensional materials with piezoelectric and ferroelectric functionalities. *npj 2D Mater. Appl.* **2018**, *2*, No. 18.
(8) Li, R.; Cheng, Y.; Huang, W. Recent progress of Janus 2D transition metal chalcogenides: from theory to experiments. *Small* **2018**, *14* (45), No. 1802091.
(9) Hwang, E.; Adam, S.; Sarma, S. D. Carrier transport in two-dimensional graphene layers. *Phys. Rev. Lett.* **2017**, *98*, No. 186806.
(10) Schwierz, F. Graphene transistors. *Nat. Nanotechnol.* **2010**, *5*, 487−496.
(11) Prezhdo, O. V. Graphene — The ultimate surface material. *Surf. Sci.* **2011**, *605*, 1607−1610.
(12) Singh, V.; Joung, D.; Zhai, L.; Das, S.; Khondaker, S. I.; Seal, S. Graphene based materials: Past, present and future. *Prog. Mater. Sci.* **2011**, *56*, 1178−1271.
(13) Naguib, M.; Mashtalir, O.; Carle, J.; Presser, V.; Lu, J.; Hultman, L.; Gogotsi, Y.; Barsoum, M. W. Two-dimensional transition metal carbides. *ACS Nano* **2012**, *6*, 1322−1331.
(14) Dahlqvist, M.; Alling, B.; Rosen, J. Stability trends of MAX phases from first principles. *Phys. Rev. B* **2010**, *81*, No. 220102.
(15) Naqvi, S. R.; Shukla, V.; Jena, N. K.; Luo, W.; Ahuja, R. Exploring two-dimensional M_2NS_2 (M = Ti, V) MXenes based gas sensors for air pollutants. *Appl. Mater. Today* **2020**, *19*, No. 100574.
(16) Aslam, M. K.; Niu, Y. B.; Xu, M. W. MXenes for non-lithium-ion (Na, K, Ca, Mg, and Al) batteries and supercapacitors. *Adv. Energy Mater.* **2020**, *11*, No. 2000681.
(17) Kim, H.; Wang, Z. W.; Alshareef, H. N. MXetronics: electronic and photonic applications of MXenes. *Nano Energy* **2019**, *60*, 179−197.
(18) Xie, Y.; Naguib, M.; Mochalin, V. N.; Barsoum, M. W.; Gogotsi, Y.; Yu, X.; Nam, K. W.; Yang, X. Q.; Kolesnikov, A. I.; Kent, P. R. C. Role of surface structure on Li-ion energy storage capacity of two-dimensional transition-metal carbides. *J. Am. Chem. Soc.* **2014**, *136*, 6385−6394.
(19) Su, X.; Guo, R. G.; Xu, S.; Wang, S. J.; Li, X. H.; Cui, H. L. Influence of O-vacancy concentration on the structural, electronic properties and quantum capacitance of monolayer Ti_2CO_2: A first-principles study. *Vacuum* **2022**, *196*, No. 110740.
(20) Li, X. H.; Liu, M. Z.; Tan, X. M.; Su, X.; Guo, R. G.; Zhang, R. Z.; Cui, H. L. Influence of C-vacancy-line defect on electronic and optical properties and quantum capacitance of Ti_2CO_2 MXene: A first-principles study. *J. Phys. Chem. Solids* **2023**, *176*, No. 111254.
(21) Li, X. H.; Li, S. S.; Yong, Y. L.; Zhang, R. Z. Adsorption of NH_3 onto vacancy-defected Ti_2CO_2 monolayer by first principles calculations. *Appl. Surf. Sci.* **2020**, *504*, No. 144325.
(22) Zhang, X.; Zhang, Z.; Li, J.; Zhao, X.; Wu, D.; Zhou, Z. Ti_2CO_2 MXene: a highly active and selective photocatalyst for CO_2 reduction. *J. Mater. Chem. A* **2017**, *5*, 12899−12903.
(23) Yu, X.-f.; Cheng, J.; Liu, Z.; Li, Q.; Li, W.; Yang, X.; Xiao, B. The band gap modulation of monolayer Ti_2CO_2 by strain. *RSC Adv.* **2015**, *5*, 30438−30444.
(24) Zhang, Y.; Zha, X.; Luo, K.; Qiu, N.; Zhou, Y.; He, J.; Chai, Z.; Huang, Z.; Huang, Q.; Liang, Y.; Du, S. Tuning the electrical conductivity of Ti_2CO_2 MXene by varying the layer thickness and applying strains. *J. Phys. Chem. C* **2019**, *123*, 6802−6811.
(25) Lai, S.; Jeon, J.; Jang, S. K.; Xu, J.; Choi, Y. J.; Park, J. H.; Hwang, E.; Lee, S. Surface group modification and carrier transport properties of layered transition metal carbides (Ti_2CT_x, T: − OH, − F and − O). *Nanoscale* **2015**, *7*, 19390−19396.
(26) Kresse, G.; Furthmüller, J. Efficient iterative schemes for *ab initio* total-energy calculations using a plane-wave basis set. *Phys. Rev. B* **1996**, *54*, 11169−11186.
(27) Kresse, G.; Joubert, D. From ultrasoft pseudopotentials to the projector augmented-wave method. *Phys. Rev. B* **1999**, *59*, 1758−1775.
(28) Perdew, J. P.; Burke, K.; Ernzerhof, M. Generalized gradient approximation made simple. *Phys. Rev. Lett.* **1996**, *77*, 3865−3868.
(29) Togo, A.; Oba, F.; Tanaka, I. First-principles calculations of the ferroelastic transition between rutile-type and $CaCl_2$-type SiO_2 at high pressures. *Phys. Rev. B* **2008**, *78*, No. 134106.
(30) Baroni, S.; de Gironcoli, S.; Dal Corso, A.; Giannozzi, P. Phonons and related crystal properties from density-functional perturbation theory. *Rev. Mod. Phys.* **2001**, *73*, No. 515.
(31) van de Walle, A.; Ceder, G. The effect of lattice vibrations on substitutional alloy thermodynamics. *Rev. Mod. Phys.* **2002**, *74*, 11−45.
(32) Madsen, G. K. H.; Singh, D. J. BoltzTraP. A code for calculating band-structure dependent quantities. *Comput. Phys. Commun.* **2006**, *175*, 67−71.
(33) Zhao, S.; Kang, W.; Xue, J. MXene nanoribbons. *J. Mater. Chem. C* **2015**, *3*, 879−888.
(34) Feng, L.; Zha, X. H.; Luo, K.; Huang, Q.; He, J.; Liu, Y.; Deng, W.; Du, S. Structures and mechanical and electronic properties of the Ti_2CO_2 MXene incorporated with neighboring elements (Sc, V, B and N). *J. Electron. Mater.* **2017**, *46*, 2460−2466.
(35) Hadipour, H.; Yekta, Y. *Ab initio* study of the effective Coulomb interactions and Stoner ferromagnetism in M_2C and M_2CO_2 MXenes (M = Sc, Ti, V, Cr, Fe, Zr, Nb, Mo, Hf, Ta). *Phys. Rev. B* **2019**, *100*, No. 195118.
(36) Delley, B. From molecules to solids with the Dmol3 approach. *J. Chem. Phys.* **2000**, *113*, 7756−7764.
(37) Huang, L. F.; Gong, P. L.; Zeng, Z. Correlation between structure, phonon spectra, thermal expansion, and thermomechanics of single-layer MoS_2. *Phys. Rev. B* **2014**, *90*, No. 045409.
(38) Huang, L. F.; Zeng, Z. Lattice dynamics and disorder-induced contraction in functionalized graphene. *J. Appl. Phys.* **2013**, *113*, No. 083524.
(39) Mounet, N.; Marzari, N. First-principles determination of the structural, vibrational and thermodynamic properties of diamond, graphite, and derivatives. *Phys. Rev. B* **2005**, *71*, No. 205214.
(40) Champagne, A.; Shi, L.; Ouisse, T.; Hackens, B.; Charlier, J. C. Electronic and vibrational properties of V_2C-based MXenes: From experiments to first-principles modeling. *Phys. Rev. B* **2018**, *97*, No. 115439.
(41) Liu, P. F.; Bo, T.; Xu, J.; Yin, W.; Zhang, J.; Wang, F.; Eriksson, O.; Wang, B. First-principles calculations of the ultralow thermal conductivity in two-dimensional group-IV selenides. *Phys. Rev. B* **2018**, *98*, No. 235426.
(42) Huang, L. F.; Cao, T. F.; Gong, P. L.; Zeng, Z. Isotope effects on the vibrational, Invar, and Elinvar properties of pristine and hydrogenated graphene. *Solid State Commun.* **2014**, *190*, 5−9.
(43) Lai, S.; Jeon, J.; Jang, S. K.; Xu, J.; Choi, Y. J.; Park, J. H.; Hwang, E.; Lee, S. Surface group modification and carrier transport properties of layered transition metal carbides (Ti_2CT_x, T: -OH, -F and = O). *Nanoscale* **2015**, *7*, 19390−19396.
(44) Frodelius, J.; Bjork, E. M.; Cordoba, J. M.; Oden, M.; Eklund, P.; Hultman, L. Annealing of Thermally Sprayed Ti_2AlC Coatings. *Int. J. Appl. Ceram. Technol.* **2011**, *8*, 74−84.
(45) Khazaei, M.; Arai, M.; Sasaki, T.; Estili, M.; Sakka, Y. Two-dimensional molybdenum carbides: potential thermoelectric materials of the MXene family. *Phys. Chem. Chem. Phys.* **2014**, *16*, 7841−7849.
(46) Gandi, A. N.; Alshareef, N. H.; Schwingenschlögl, U. Thermoelectric performance of the MXenes M_2CO_2 (M = Ti, Zr, or Hf). *Chem. Mater.* **2016**, *28*, 1647−1652.
(47) Li, T. Ideal strength and phonon instability in single-layer MoS_2. *Phys. Rev. B* **2012**, *85*, No. 235407.
(48) Zha, X. H.; Yin, J.; Zhou, Y.; Huang, Q.; Luo, K.; Lang, J.; Francisco, J. S.; He, J.; Du, S. Intrinsic structural, electrical, thermal, and mechanical properties of the promising conductor Mo_2C MXene. *J. Phys. Chem. C* **2016**, *120*, 15082−15088.
(49) Zhang, S. H.; Zhou, J.; Wang, Q.; Chen, X. S.; Kawazoe, Y.; Jena, P. Penta-graphene: a new carbon allotrope. *Proc. Nati. Acad. Sci. U.S.A.* **2015**, *112*, 2372−2377.
(50) Yorulmaz, U.; Özden, A.; Perkgöz, N. K.; Ay, F.; Sevik, C. Vibrational and mechanical properties of single layer MXene

https://doi.org/10.1021/acsomega.3c08540
ACS Omega 2023, 8, 48549−48556

structures: a first principles investigation. *Nanotechnology* **2016**, *27*, No. 335702.
(51) Lee, C.; Wei, X.; Kysar, J. W.; Hone, J. Measurement of the elastic properties and intrinsic strength of monolayer graphene. *Science* **2008**, *321* (5887), 385−388.
(52) Andrew, R. C.; Mapasha, R. E.; Ukpong, A. M.; Chetty, N. Mechanical properties of graphene and boronitrene. *Phys. Rev. B* **2012**, *85* (12), No. 125428.
(53) Bertolazzi, S.; Brivio, J.; Kis, A. Stretching and breaking of ultrathin MoS_2. *ACS Nano* **2011**, *5* (12), 9703−9709.
(54) Lv, S. J.; Yin, G. X.; Cui, H. L.; Wang, H. Y. Electronic, vibrational, elastic, and piezoelectric properties of H-, F-functionalized AlN sheets. *Phys. Status Solidi (B)* **2021**, *258*, No. 2100216.
(55) Castro Neto, A. H.; Guinea, F.; Peres, N. M. R.; Novoselov, K. S.; Geim, A. K. The electronic properties of graphene. *Rev. Mod. Phys.* **2009**, *81*, No. 109.
(56) Jiang, J. W. Graphene versus MoS_2: A short review. *Front. Phys.* **2015**, *10* (3), 287−302.
(57) Sevik, C. Assessment on lattice thermal properties of two-dimensional honeycomb structures: Graphene, h-BN, h-MoS2, and h-MoSe2. *Phys. Rev. B* **2014**, *89*, No. 035422.

https://doi.org/10.1021/acsomega.3c08540
ACS Omega 2023, 8, 48549−48556